nature communications

Article

https://doi.org/10.1038/s41467-025-59545-0

Structures of native SV2A reveal the binding mode for tetanus neurotoxin and anti-epileptic racetams

Received: 10 August 2024

Accepted: 24 April 2025

Published online: 05 May 2025

Check for updates

Stephan Schenck[1,2,3], Toon Laeremans[1,2], Jan Steyaert[1,2] & Janine D. Brunner[1,2,3]

The synaptic vesicle glycoprotein 2A (SV2A) is a synaptic vesicle (SV) resident with homology to the major facilitator superfamily (MFS) and essential in vertebrate neurotransmission. Despite its unclear physiological role, SV2A is of high medical relevance as it is the target of the anti-epileptic drug Levetiracetam (LEV) and a receptor for clostridial neurotoxins (CNTs), among them presumably tetanus neurotoxin (TeNT). To obtain detailed insights about these molecular interactions we subjected native SV2A, purified from brain tissue, to cryo-EM. We discover that TeNT binds SV2A strikingly different from botulinum neurotoxin A and unveil the precise geometry of TeNT binding to dipartite SV2-ganglioside receptors. The structures deliver compelling support for SV2A as the protein receptor for TeNT in central neurons and reinforce the concepts of the dual receptor hypothesis for CNT entry into neurons. Further, our LEV-bound structure of SV2A reveals the drug-interacting residues, delineates a putative substrate pocket in SV2A and provides insights into the SV2-isoform-specificity of LEV. Our work has implications for CNT engineering from a hitherto unrecognized SV2 binding interface and for improved designs of anti-convulsant drugs in epilepsy treatment.

Synaptic vesicles (SVs) store neurotransmitters for release into the synaptic cleft upon fusion with the presynaptic membrane and are among the best-studied organelles in the cell[1]. Yet, several SV residents have resisted efforts to unveil their precise function. Among those proteins is the synaptic vesicle glycoprotein 2 family (SV2), consisting of three members, SV2A-C in vertebrate genomes[2,3]. SV2A, cloned more than 30 years ago[4,5], is a multi-pass membrane protein with MFS architecture and strict SV-localization. It is the most widely expressed isoform in the brain where it is found in inhibitory and excitatory neurons. In early studies SV2A was proposed to constitute a transporter due to substantial homology to sugar transporters[4,5]. It was further considered as a regulator of presynaptic Ca^{2+} levels where it was suggested that SV2A/B achieve this through uptake of Ca^{2+} into SVs[6]. However, a substrate, potentially even a neurotransmitter or modulator, could not be assigned to SV2A (but see[7]). Further, a Ca^{2+} uptake activity into SVs by SV2 proteins could not be supported[8]. The deletion of SV2A in mice leads to severe seizures resulting in fatality within three weeks after birth, underpinning its importance in the brain[6,9]. In electrophysiological studies, it was shown that the deletion of SV2A causes reduced evoked synaptic response but basic transmission parameters like miniature frequency and amplitude as well as the size of the readily releasable pool are unaffected[10]. SV2A seems to be required in a last step of the exocytotic cycle before Ca^{2+}-elicited fusion of SVs, after docking and priming[2,10]. Rescue experiments in SV2A/B knock-out (KO) neurons have shown that conserved residues in the transmembrane moiety (Trp300 and Trp666) are required for SV2A function[11] but no clear molecular explanation could be derived from these experiments. Nevertheless, the data is in support of a transport function because the conserved residues that have been mutated localize to functionally critical regions in other MFS

[1]VIB-VUB Center for Structural Biology, VIB, Brussels, Belgium. [2]Structural Biology Brussels, Vrije Universiteit Brussel, VUB, Brussels, Belgium. [3]Structure and Function of Membrane Proteins, VIB-VUB Center for Structural Biology, VIB, Brussels, Belgium. e-mail: janine.brunner@vub.be

transporters at the core of the transmembrane domain between the N- and C-terminal halves[12]. SV2 proteins interact with the Ca^{2+}-sensor synaptotagmin (Syt)[13–15] during SV-retrieval and data from several studies suggested that reduced Syt levels in SVs are causative for the observed deficits in SV2A deletion studies[16–18] but N-terminal deletion mutants of SV2A, devoid of their Syt interaction site, could rescue the SV2A/B Double-KO (DKO) in another report[10]. SV2 proteins were further suggested to contribute to transmitter storage in SVs through attached keratan sulfates[19], but the presence of such modifications on SV2 proteins could not be supported in a recent mass-spectrometric analysis of SV proteins[20]. Importantly, many of the suggested functions of SV2 proteins are not exclusive, hence SV2 proteins could fulfill multiple roles[2,3].

Despite these many uncertainties regarding its primary function, SV2A has been identified as the target of the major anti-epileptic drug Levetiracetam (LEV)[21,22], one of the most prescribed anti-seizure medications. Mutagenesis scans of SV2A using radiolabelled racetams in binding assays revealed several relevant residues for drug binding such as Asp670, Trp300 and Trp666[23,24] of which the tryptophans were shown to be essential in rescue experiments of the SV2A KO[11]. Further, LEV was shown to reproduce some of the deficits in neurotransmission seen in SV2A/B DKO when incubated in wild-type neurons over an extended period and after trains of neuronal stimulation[25,26]. Together, these data make it plausible that LEV interferes with the function of SV2A and that bound LEV could localize to a substrate binding pocket. To address the binding site of LEV and obtain further insight into the nature of the presumed substrate binding pocket of SV2A, high-resolution structures would be required.

SV2 proteins also constitute protein receptors for botulinum neurotoxins (BoNTs)[27–29], which are together with tetanus neurotoxin (TeNT), the most potent biological toxins known[30]. SV2 proteins are the receptors for the BoNT serotypes A, C, D, E and F[27,31–37] and presumably TeNT[28,29,38], although for the latter case conflicting data have been published[39,40]. Tetanus has been a major burden for the largest part of human history and remains a cause for neonatal death in less vaccinated regions of the world, yet the mechanism of entry into central neurons (i.e. into inhibitory interneurons in the anterior horn of the spinal cord) has remained unclear. TeNT recognizes lipidic (i.e. gangliosides)[41–44] and one or more proteinaceous receptors, like the other CNTs. The search for protein receptors is also complicated due to the peculiar pathway of TeNT to reach its targeted neurons[45]: The toxin enters first motor neurons, and reaches the postsynaptic endings of these peripheral neurons by retrograde trafficking inside endosomal structures. TeNT is then released into the synaptic cleft and enters presynaptic central neurons, but different from the entry into motor neurons, now by endocytosis into SVs. Subsequently, the toxic light chain (LC) is unloaded through the translocation domain (H_N) into the cytosol. Recently, Nidogens, extracellular matrix proteins, were reported as receptors for TeNT at neuromuscular junctions[46,47]. For central neurons, Thy-1, a GPI-anchored glycoprotein enriched in lipid rafts in neurons, was proposed as a receptor for TeNT[48] but other data supported SV2A and SV2B as TeNT receptors[38]. These latter findings have been questioned because a preincubation of stimulated neurons with the receptor binding domain (H_C) of TeNT (TeNT-H_C) did not compete with binding of BoNT/A-H_C for neuronal entry[39]. However, this finding could probably be explained if TeNT was not binding to the same (or an overlapping) site on SV2 as BoNT/A.

We aim to advance the molecular characterization of the essential SV-resident SV2A to address the binding of the anti-epileptic drug LEV as well as contribute to our understanding of TeNT protein receptor recognition on central neurons. Here, we report cryo-EM structures of SV2A in complex with TeNT, unveiling an unknown binding site on SV2A and the simultaneous binding of co-purified endogenous gangliosides by the toxin. Further, we provide a structure of LEV-bound SV2A that reveals the binding of the drug into a substrate pocket in an outward-open conformation of SV2A, involving functionally essential residues.

Results

Purification of native SV2A

We evaluated previously generated nanobodies (Nbs) against rat/human SV2A (see Methods), for their potential to purify native SV2A from brain detergent extracts by immunoaffinity as this would also ensure native glycosylation patterns on the protein. First, we converted the Nbs into twin-StrepTagged Pro-Macrobodies[49] (Supplementary Fig. 1A, "Methods") to serve also as larger fiducial marker for improved classification in cryo-EM processing. The tagged PMbs were preloaded on Streptactin resin and incubated with mouse brain detergent extracts to bind SV2, which was co-eluted with the PMbs by application of biotin (Supplementary Fig. 1D). None of the tested Nbs bound SV2B or SV2C, but only SV2A (Supplementary Fig. 1C). SV2A is highly conserved across vertebrate species (Supplementary Fig. 1B and 3), hence we could purify SV2A from larger domestic animals (see section "Methods" and Supplementary Fig. 2) to investigate relevant molecular interactions of SV2A that are conserved across mammalian species including humans. We purified three different SV2A-PMb complexes from sheep (*Ovis aries*) brain (Supplementary Fig. 1E) and subjected them to cryo-EM analysis.

Analysis of SV2A-PMb complexes and identification of an SV2A-PMb-TeNT-H_C complex

The obtained maps provided information about the recognized epitopes on SV2A (Supplementary Fig. 1F). For SV2A-PMb2 and SV2A-PMb1 the resolution was limited to ~5.8 and 4.1 Å, respectively. Both PMbs occupied the C-terminal end of the luminal domain 4 (LD4), the site that is also bound by BoNT/A1 and BoNT/A2[31,32,50–52]. For the SV2A-PMb5 complex we could initially not obtain clear 2D-classes, and thus could not localize the epitope for this Nb. We suspected that PMb5 binds to a flexible, potentially cytosolic epitope and that the LD4 is also inherently flexible. We thus considered the SV2A-PMb5 complex as good starting material to investigate complex formation with receptor binding domains (the non-toxic C-terminal domains of the toxin's heavy chain, H_C) of BoNT/A1 and TeNT. When the SV2A-PMb5 complex was incubated with the H_C of BoNT/A1 or TeNT (TeNT-H_C) we observed co-elution of the SV2A-PMb5 complex with TeNT-H_C in SEC, but not of BoNT/A1-H_C (Supplementary Fig. 4A, B). The tripartite complex containing TeNT-H_C was subjected to cryo-EM and we obtained a map resolved to a global resolution of 3.25 Å (~2.9 Å in the TM part) (Fig. 1A, Supplementary Table 1, Supplementary Figs. 5 and 6A). TeNT-H_C appears to stabilize movements in the LD4 substantially. Further processing of data from the dipartite SV2A-PMb5 complex revealed that PMb5 becomes discernible also in the absence of TeNT-H_C albeit at lower resolution and requiring long collection times, explaining why it initially escaped our analysis (Supplementary Fig. 1F). The map of the tripartite complex resolves PMb5 and TeNT-H_C unambiguously and shows that PMb5 binds on the C-terminal end of the LD4, similar to PMb1 (Supplementary Fig. 1F), whereas TeNT-H_C was clearly resolved on the N-terminal end. The occupation of the C-terminal site on the LD4 by PMb5 readily explains why we could not form a complex with BoNT/A1H_C which otherwise could bind to SV2A[27].

The structure of SV2A in the SV2A-PMb5-TeNT-H_C complex

The N-terminal cytosolic 144 amino acids (AA) of SV2A, a region to which Syt binds, were not resolved and may thus be natively unstructured, like in the predicted fold. The rest of the protein sequence, except for two flexible loops (AA 323-329 and 401-420), could be unambiguously assigned to the map to build a model (Fig. 1A, B). SV2A features an architecture reminiscent of many MFS transporters with twelve transmembrane (TM) helices of which the N-terminal 6 TM helices are pseudo-symmetrically related to the

https://doi.org/10.1038/s41467-025-59545-0

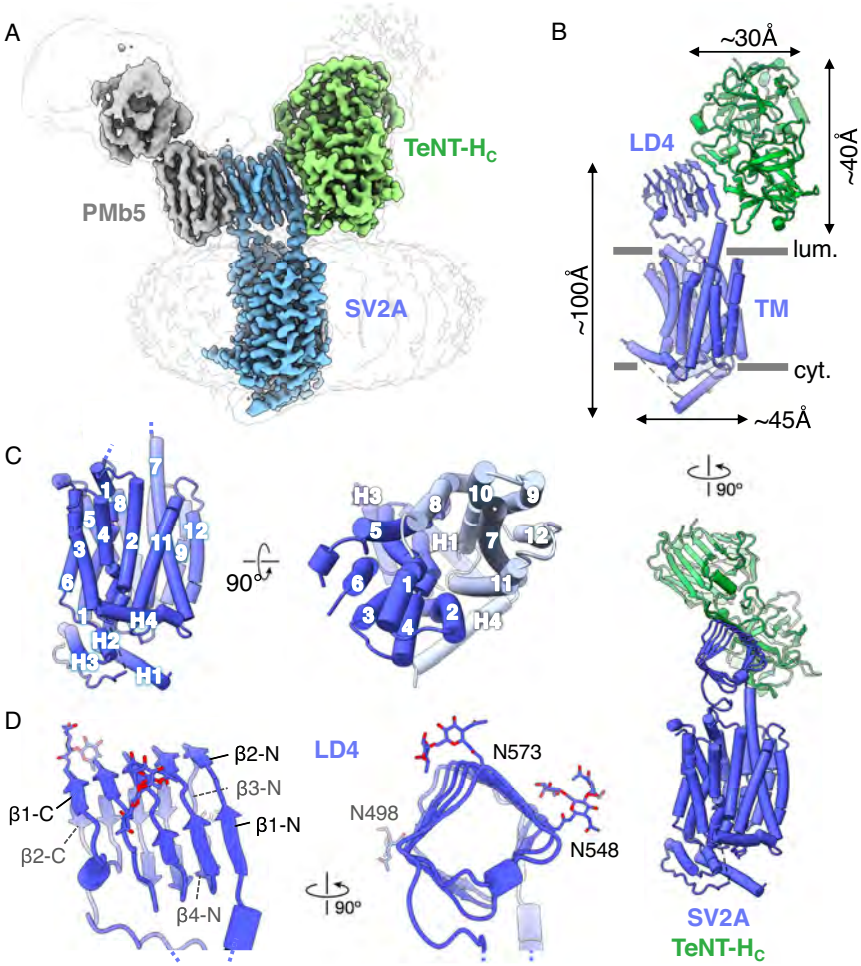

Fig. 1 | The cryo-EM structure of native sheep SV2A in a ternary complex with PMb5 and TeNT-H$_C$. **A** Cryo-EM map of SV2A (blue) at a resolution of 3.25 Å with bound PMb5 (gray) and TeNT-H$_C$ (green). The micelle is outlined in light gray. The map was contoured at 0.12σ in ChimeraX. **B** Model with dimensions of the SV2A-TeNT-H$_C$ complex viewed from the sides. Cyt.: cytosolic, Lum.: luminal. **C** Transmembrane part of SV2A with numbered helices from the side and a top view from luminal (N- and C-halves colored in blue and gray, respectively). **D** The SV2A-LD4 with relevant β-strands labeled and showing the N-glycans. Viewed from the side and along its longitudinal axis (from C-terminal to N-terminal).

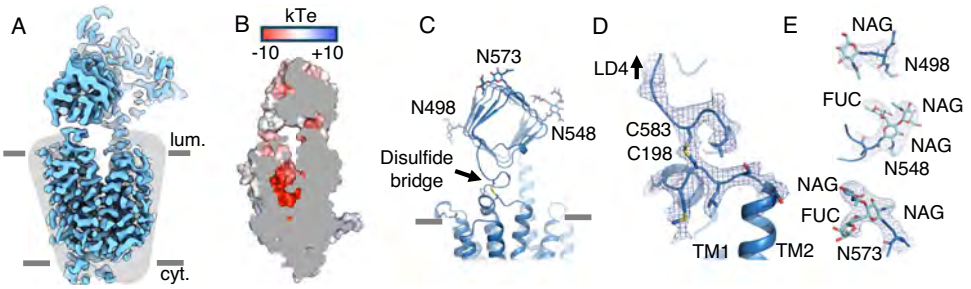

Fig. 2 | Structural features of SV2A. **A** Cryo-EM map of SV2A showing the outward-open conformation with the two halves (N- and C-) indicated as gray shadows. Cyt.: cytosolic, Lum.: luminal. **B** Surface electrostatics as calculated with APBS showing an overall negative charge (red) in the transmembrane cavity between the N- and C-halves of the TM part. **C** The luminal SV2A-LD4 with the disulfide bridge between Cys198 (loop between TM helices 1 and 2) and Cys583 (preceding TM helix 8) and the resolved N-glycans as viewed from its C-terminal end. **D** Density map and model of the luminal disulfide bridge. **E** Density map and models of the protein-proximal ends of the N-glycans at the three N-linked glycosylation sites of SV2A - Asn498, Asn548 and Asn 573. One to two NAG units and α-1-6-glycosidic-bonded fucose are modeled. In (**D**) and (**E**) the filtered map is shown at a contour level of 9 and 8σ (Pymol), respectively.

C-terminal half (Fig. 1C, Supplementary Fig. 7A). SV2A is captured in an outward open state (Supplementary Fig. 13) characterized by a cavity between the N-terminal and C-terminal halves that opens to the luminal (or extracellular) side and is roofed by the LD4 (Fig. 2A). The cavity is lined by TM helices 1,2,4 and 5 on the N-terminal half and 7,8,10 and 11 on the C-terminal half and extends to the functionally relevant residues Trp300 (TM helix 5) and Trp666 (TM helix 10)[11] which are also involved in LEV binding (Fig. 1C)[22–24]. The electrostatic potential of the cavity is negative as analyzed with APBS (Fig. 2B). This negative potential could serve an attraction of positively charged

solutes or ions, e.g. protons. On the cytosolic face, SV2A features a characteristic helix (H1) before the TM part that is extended in parallel to the membrane surface and in close apposition to the lipids of the membrane. Three additional helices after TM helix 6 in a loop between the N- and C-terminal halves are arranged like a triangle with H4 positioned nearly 90° relative to H1 (Fig. 1B, C).

The LD4 is a unique domain that is present in all three isoforms of SV2 and forms a quadrilateral β-helix (Fig. 1D, Supplementary Fig. 7A) as seen in bacterial penta-peptide repeat proteins[53,54] but in no other transporter in humans. Its structure was previously solved as isolated domain (from SV2C or as chimeric SV2C/A version[31,32,37]). The LD4 is connected to the TM part through the C-terminus of helix 7 and the N-terminus of helix 8. An additional anchorage point is formed through a disulfide bridge between Cys198 after TM helix 1 and Cys583 at the C-terminal end of LD4, preceding TM helix 8 as judged from the clear density in our map (Fig. 2C, D). These cysteines are highly conserved across species and all isoforms in support of a functional importance in SV2 proteins (Supplementary Fig. 3, 7B, and 12). Despite the multiple connections to the transmembrane domain, we conclude that the LD4 is relatively flexible from the maps with different PMbs. The function of this domain remains unclear, but a regulatory function appears possible as the LD4 is connected directly to the cavity-lining TM helices 7 and 8 and additionally to TM helices 1 and 2 through the disulfide bridge. The domain could thus influence four TM helices in their movements and positions and thereby impact a transport function. In the map we noted a density that reaches from the N-terminal end into the hydrophobic interior (Phe-repeats) of the LD4 and that likely represents a DDM molecule (Supplementary Fig. 7C). Hydrophobic substances would be prone to bind there, but whether the LD4 is a binding site for hydrophobic molecules is currently difficult to state.

We noticed that SV2A does not reside in the center of the micelle (Supplementary Fig. 7D). This feature is obvious from our maps irrespective of the PMb bound or whether the TeNT-H_C is present. We could not find any additional density originating from a transmembrane binding partner that could cause the asymmetric position of SV2A in the micelle. A mass spectrometric analysis of gel bands of copurified proteins (Supplementary Fig. 7E) did also not hint to established transmembrane binding partners, such as Syts[55]. SV2A has been described as highly glycosylated protein, hence its name. The glycosylation was suggested to be involved in transmitter storage[19] and is enhancing the binding of BoNT/A[32]. We could identify the protein-proximal part of three N-glycans on the LD4 with N-Acetylglucosamine (NAG) groups attached to Asn498, Asn548 and Asn573 that are fucosylated, which has also been reported recently in a mass-spectrometric analysis of SV2A[20]. A second NAG can be resolved for the glycan at Asn548 and Asn573. (Figs. 1D, and 2C, E). We do not see densities for very large structures like keratan-sulfates, that have been proposed for SV2 proteins[2,19], but keratan sulfate-I could not be excluded as the protein-proximal part of these structures has an identical composition to common N-glycans. A recent mass-spectrometric analysis of SV2A refuted however the presence of keratan sulfates on SV2A[20].

TeNT-H_C binds SV2A on the N-terminal end of the LD4 by parallel β-strand augmentation

Unexpectedly, TeNT-H_C is bound to the N-terminal end of the LD4 domain of SV2A through an extended interface of the β-hairpin of the TeNT-H_C with the exposed β-strand of the LD4 in parallel arrangement by β-sheet augmentation (Fig. 3A, B). Although reminiscent of the binding mode of BoNTs A1 and A2, TeNT-H_C binds to an open-ended β-strand of the LD4 (β2-N) in opposite direction and not by anti-parallel β-sheet formation seen for BoNT/A1 and A2 (Fig. 3D, Supplementary Fig. 7A). While it appears in principle plausible for CNTs to bind also on the N-terminal end of the LD4, there has been no case described yet. The TeNT-H_C forms four hydrogen bonds between the β-hairpin through main-chain interactions to extend the β-sheet in parallel fashion. Serine1156_{TeNT}, Tyr1157_{TeNT}, Thr1158_{TeNT} and Gly1160_{TeNT} interact with the β2-N strand of LD4 (Arg491_{SV2A} and Glu493_{SV2A}) (Fig. 3B). Additional side-chain interactions contribute to the binding: Glu493_{SV2A} with Tyr1157_{TeNT} and Asn1159_{TeNT}, His494_{SV2A} with Asn1159_{TeNT} as well as the carbonyl oxygen of Gly489_{SV2A} and Arg1168_{TeNT} (Fig. 3B). In addition, there is a hydrogen bond between the carbonyl oxygen of Ala482_{SV2A} with Asn1280_{TeNT}. We see no interactions with the three N-glycans on the LD4 domain that would contribute to the binding of TeNT-H_C to SV2A. This is in line with previous mutagenesis studies[38] and in contrast to the glycan-H_C interactions described for BoNT/A[32]. TeNT also binds SV2B but not SV2C[38], even though the β2-N stretch is not conserved between SV2A and SV2B (Supplementary Fig. 12). This should affect the side-chain interactions, but His434_{SV2B} (corresponding to Arg491_{SV2A}) could instead interact with Arg1168_{TeNT}. Tyr436_{SV2B} is located at the position of Glu493_{SV2A}, which is involved in a network of hydrogen bonds (Fig. 3B). Presumably, Tyr436_{SV2B} could form other hydrogen bonds (e.g. with Tyr1157_{TeNT} or Asn1159_{TeNT}) which would compensate the absence of a glutamate at this position. A similar scenario is known for the side chain interactions of BoNT/A1 and BoNT/A2 with the SV2C-LD4[31,50,51] where the difference in the sequences indicates a high tolerance for substitutions of binding residues. Regarding SV2C, a difference in the Cα-trace at the LD4 could account for the lack of interaction. The Alphafold-2[56] (AF2) models of the SV2B/C isoforms show that the β2-N strand of the SV2C-LD4 differs significantly from SV2A and SV2B (Fig. 3C) which provides a possible explanation for the lack of interaction between TeNT and SV2C. Isolated, recombinantly expressed LD4 of SV2C[32,50,51] and an SV2A/C chimera[37] are not forming the same quadrilateral arrangement of the β-strands at the N-terminus of the LD4 (β1-N is not formed, β2-N incomplete) different from what is seen in the full-length SV2A protein (Supplementary Fig. 4C). Consequently, the binding of a CNT (i.e. TeNT) to the N-terminal end of an LD4 is apparently only possible with full-length SV2 protein. We subjected also an SV2A-PMb1-TeNT-H_C complex to cryo-EM and revealed identical binding of TeNT-H_C on the N-terminus of LD4 (Supplementary Fig. 4D), ruling out an artefactual state caused by PMb5. Supplementary Fig. 4E shows an overlay of the TeNT-holoenzyme[44] with our SV2A-TeNT-H_C structure. Notably, a BoNT/A holoenzyme could also bind to a TeNT-occupied SV2A-LD4, at least in this static snapshot.

Co-purified complex gangliosides are bound by TeNT-H_C in the complex with SV2A

TeNT binds to gangliosides through two independent binding sites (which was also reported for BoNT/C[57]), the R-site (Arg1226_{TeNT}) and the W-site (Trp1289_{TeNT}) on the TeNT-H_C[41–44]. Whether these two sites are occupied by complex gangliosides at the same time is less clear[28]. We recognized two unambiguous densities that extend from the detergent micelle into the R- and W-sites (Fig. 4A) and could fit the carbohydrate moieties of two gangliosides into the densities after a focused refinement (Supplementary Fig. 6C, Supplementary Table 1). The best fit for the density at the R-site is GD2 and for the W-site it is GD1a (Fig. 4B–D). GD3, GT3, GT2 and GD2 gangliosides were reported to bind into the R-site[41]. For the W-site, GM1a, GT1b and GD1a were identified as binders[42,44]. Our data are thus in good agreement with previous results. The central interaction in the W-site pocket is achieved through planar interactions of the distal (second) galactose unit with Trp1289. Trp1289 is further aligned and stabilized in its position by π-interactions with Tyr1290 and His1293. The same galactose unit is hydrogen-bonded by His1271 and the backbone carbonyl oxygen of Thr1270. Additional interactions with GD1a are mediated through hydrogen bonds of Asn1219 and Asp1222 with the N-acetyl-D-galactosamine unit (Fig. 4B). The interactions of TeNT with GD1a are very similar to the ones seen in a crystal structure[44], although some interactions are not present in our structure (Trp1289 with a

https://doi.org/10.1038/s41467-025-59545-0

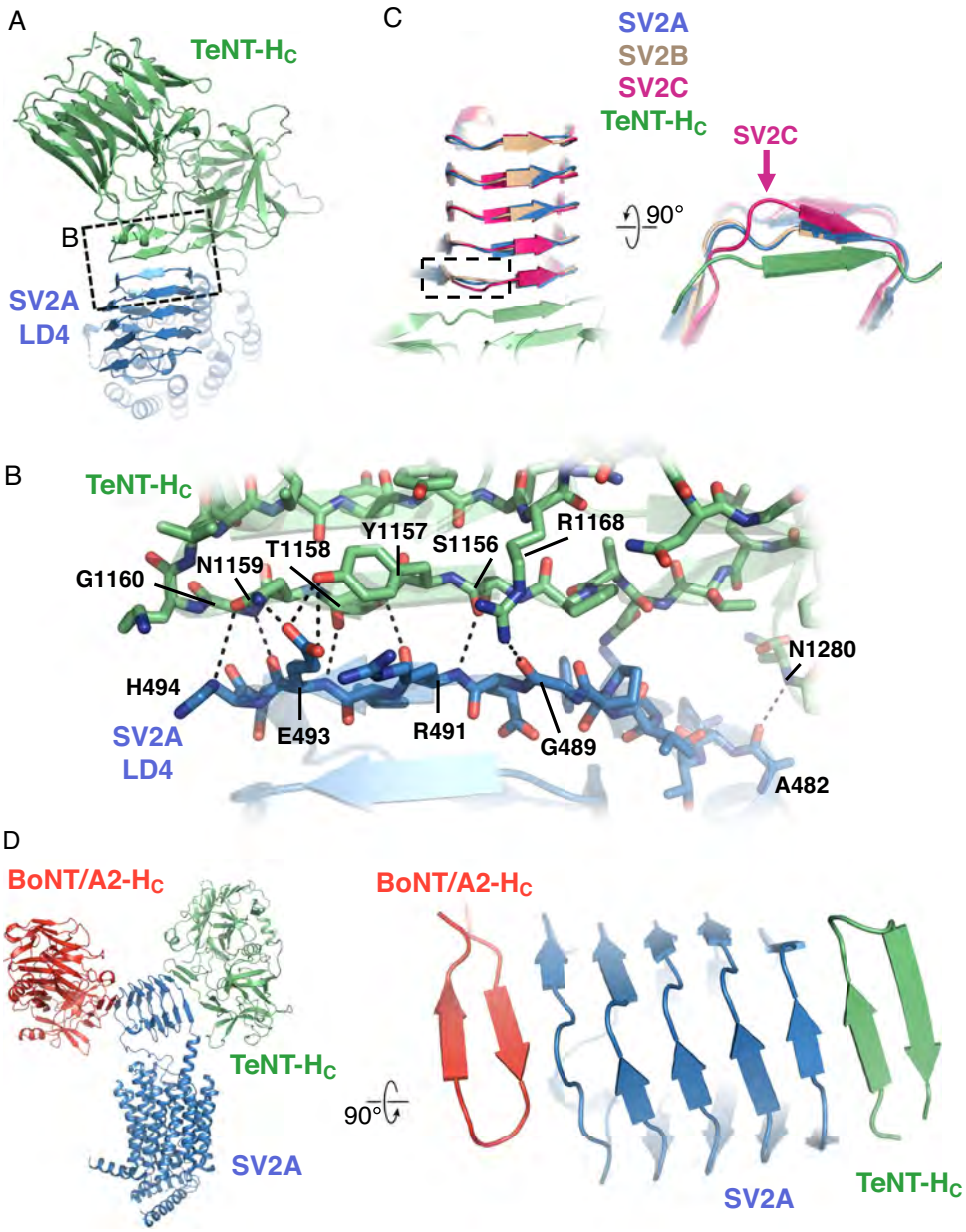

Fig. 3 | TeNT-H_C interactions with SV2A. A Top view from luminal on the interface of TeNT-H_C (green) and the SV2A LD4 (blue), showing the parallel beta-strand orientation of the TeNT-H_C β-hairpin bound to β2-N of the LD4. **B** Enlarged view of boxed area in (A) depicting residues of β2-N of SV2A-LD4 (blue) and the β-hairpin of TeNT-H_C (green) that contribute to the binding and the formation of a parallel β-sheet. Main chain- and side chain-interactions shown with black dashed lines. **C** AF2-models of the LD4 of human SV2C (pink), human SV2B (wheat) aligned with the sheep SV2A cryo-EM structure (SV2A in blue, TeNT-H_C in green) seen from top and turned by 90° viewed onto the N-terminal side and including the first strand of the TeNT-H_C β-strand. The SV2C β2-N strand shows a deviating trajectory (indicated with a pink arrow). **D** BoNT/A2-H_C (orange) in complex with SV2A-LD4 (8JLG) was aligned through the LD4 domain to the SV2A-TeNT-H_C complex in blue and green. The SV2A LD4 from 8JLG is omitted for clarity. View from top (right panel) shows the antiparallel orientation of the BoNT/A2-H_C β-hairpin at the C-terminus of the LD4 and the parallel β-sheet formation between the TeNT-H_C β-hairpin and the SV2A LD4.

carboxy group of N-acetyl-neuraminic acid (NeuAc) in the PDB entry 5N0B. A possible explanation for this is that in the previously reported X-ray structure only the oligosaccharide moiety has been applied while in our study we report the interactions with detergent-embedded gangliosides. The carbohydrate moiety of GD2 is complexed mainly through hydrogen bonds of Asn1216, Asp1147 and Arg1226 with the membrane-proximal NeuAc unit and by Tyr1229 with the terminal NeuAc (Fig. 4C). We have not added gangliosides to the purified SV2A-PMb5-TeNT-H_C complex, the lipids are thus endogenous and stem from the sheep brain membranes. The structure supports a scenario where TeNT-H_C has two functional binding sites for complex gangliosides that would be simultaneously occupied[28].

Dipartite SV2A-ganglioside receptors reveal precise angular alignment in the β-hairpin of CNTs

The H_C-domains of the different CNTs, including TeNT, are structurally very conserved. While the largest part of the H_C of BoNT/A and TeNT aligns well, a clear difference is apparent for the β-hairpins that bind to SV2 (Supplementary Fig. 8A). When the structures of BoNT/A1/A2-H_C and TeNT-H_C are aligned, the β-hairpins of a BoNT/A-H_C and a TeNT-H_C are tilted by ~35° relative to each other (Supplementary Fig. 8B). Further, this β-hairpin-tilt-angle is nearly independent of being bound to SV2[32,50,51] (and this study) or not bound to SV2[36,58]. There are only minor deviations reported[59] for BoNT/A serotypes. Interestingly, the difference of the relative angle between the N-terminal and the C-terminal β-

https://doi.org/10.1038/s41467-025-59545-0

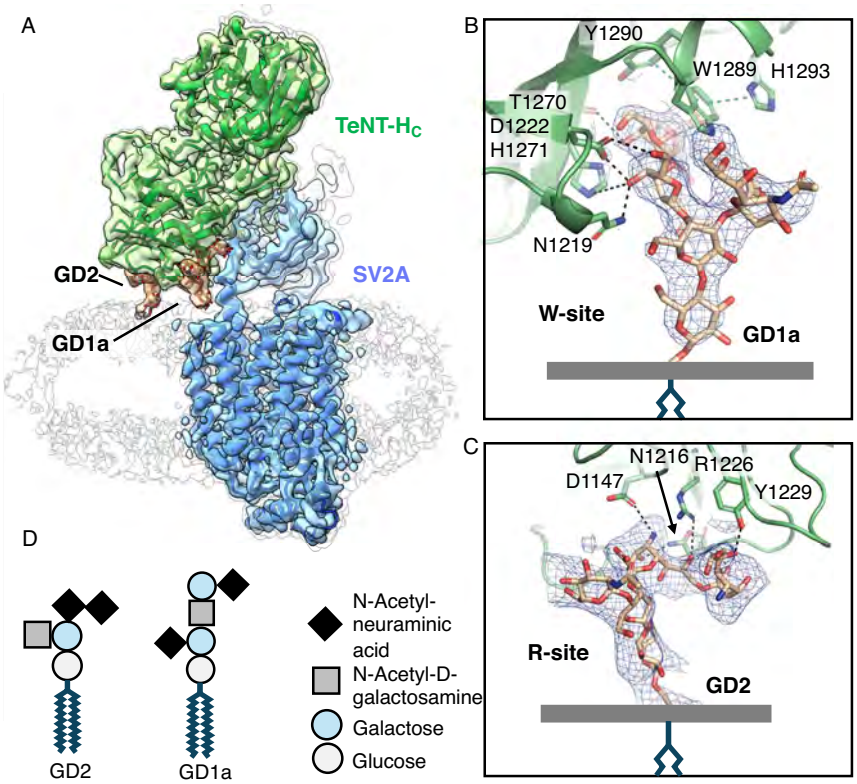

Fig. 4 | Co-purified gangliosides bound to the TeNT-H_C–SV2A complex. A Cryo-EM density map of TeNT-H_C (green) bound to SV2A (blue) and gangliosides (brown) GD1a and GD2 bound in the W- and R-sites of TeNT-H_C respectively. The detergent micelle is shown as outline in light gray. The map is contoured at a level of 5.4σ in ChimeraX. **B** Enlarged view of the density in the W-site with modeled GD1a ganglioside and TeNT-H_C (green). Residues interacting with gangliosides are shown as sticks and main interactions depicted with dashed lines (black; hydrogen bonds, cyan; π-π interactions). **C** Enlarged view of the density in the R-site with models of GD2 ganglioside (brown), and interactions as described in (**B**). In **B**, **C**, the density-modified map is contoured at 1.1 and 0.7σ in Pymol, respectively. **D** Composition and assembly of GD2 and GD1a gangliosides.

strands of the SV2A-LD4 (β2-N to β1-C) is also 30–40° as the LD4 domain is twisted along its N- to C-terminal axis. When a BoNT/A1-SV2C-LD4 (or the recent structure of BoNT/A2 bound to SV2A[52]) are aligned on our SV2A-TeNT-H_C complex (alignment centered on the LD4 domains) both H_C-domains (TeNT and BoNT/A2) show almost the same distance of the ganglioside binding sites to the membrane plane (~12 Å, as measured for the W-site, Supplementary Fig. 8C, left). Both have also a preference for the same or very similar carbohydrate moieties of gangliosides that would extend to similar degree over the membrane surface. Apparently, the angle of the β-hairpin relative to the rest of the BoNT/A-H_C and TeNT-H_C domains results in precise levelling of the ganglioside binding sites above the membrane to allow for dual binding of lipids and the LD4 at the respective ends of the LD4. The importance of this angle becomes obvious when the H_C-domains of TeNT and BoNT/A2 are exchanged and placed on the other respective ends of the LD4 (Supplementary Fig. 8C, right). For example, if TeNT-H_C is aligned to the C-terminal end of the LD4, the R- and W-sites would almost come to lie within the membrane (too low). In turn, if BoNT/A was bound at the N-terminal end, the ganglioside binding sites where too much elevated from the membrane surface (Supplementary Fig. 8C). Although, a certain flexibility in the β-hairpin and between the N- and C-terminal domains of the H_C was noticed in dependence of bound gangliosides or LD4 for BoNT/A serotypes[51,58], the reported deviations could not account for the required shift. We thus conclude that the angle of the β-hairpin has evolved to ensure binding of the respective ends of the LD4 domain of SV2 while being bound to the carbohydrate moiety of the gangliosides as illustrated in Supplementary Fig. 8.

Levetiracetam binds to SV2A in the transmembrane region in an outward-open conformation

Besides the binding of CNTs we aimed to obtain insights into the binding of the anti-epileptic racetams through a LEV-bound structure. To evaluate the capacity of our detergent-solubilized SV2A-PMb complexes to bind LEV, we subjected the purified protein to a thermal shift assay using cysteine-reactive CPM dye in a real-time PCR cycler.

With the SV2A-PMb5 sample we could observe a clear positive shift in the melting temperature (Tm) of SV2A by 3.4 °C at a LEV concentration of 250 μM (Fig. 5A, B, Supplementary Fig. 9) but not for a control protein, indicating that the SV2A-PMb-complex retained its potential to bind racetams and would be suitable for a structural approach. We subsequently obtained a cryo-EM map of SV2A-PMb5-TeNT-H_C in the presence of 250 μM LEV at 3.60Å that revealed no obvious larger differences compared to the LEV-free structure except for a clear density that is sandwiched between Trp300 and Trp666 matching to the size and shape of LEV (Fig. 5D, Supplementary Figs. 10 and 11). A focused refinement improved the resolution to 3.35 Å, and a subsequent density modification step in Phenix refined the map further (Fig. 5D, Supplementary Table 1, Supplementary Figs. 6B, D, 10 and 11A, B). From the side, in a sliced view, LEV locates to a negatively charged pocket that lies in the middle of the membrane (Fig. 5C). The space in the pocket from LEV to the luminal entry stays unperturbed and accessible for a molecule with the size of LEV. The tyrosine residues 461 and 462 (di-tyrosine motif) narrow the path for LEV towards the extracellular space, yet the space is apparently wide enough for LEV to diffuse to the pocket, because the position of this di-tyrosine motif is nearly identical in the Apo-structure (Supplementary

https://doi.org/10.1038/s41467-025-59545-0

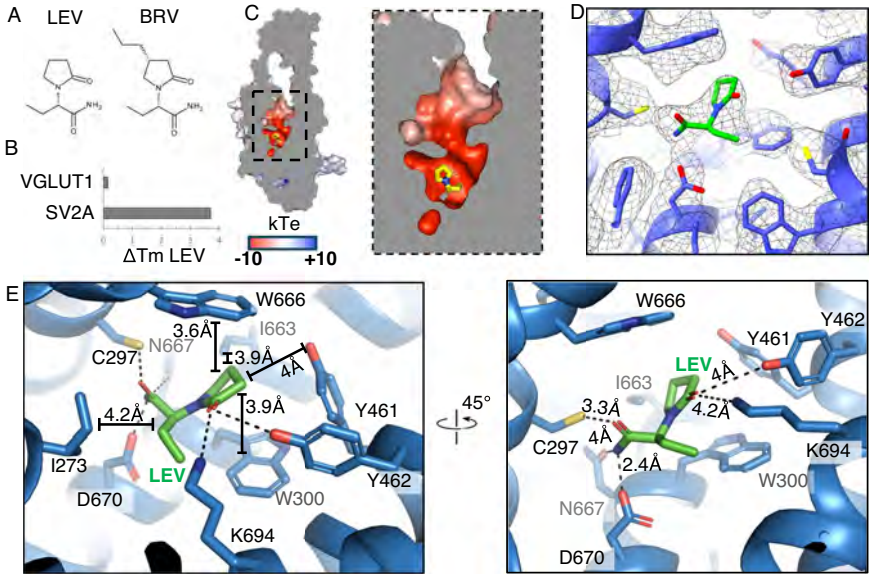

Fig. 5 | The Levetiracetam binding site in SV2A. A Chemical structure of levetiracetam (LEV) and Brivaracetam (BRV). **B** Elevation of the melting temperature (Tm) of SV2A in the presence of 250 μM LEV. The melting temperature of a control protein (rat VGLUT1) is not affected by LEV. The ΔTm shown is the mean difference of Tm between $n = 3$ technical replicates in the presence and absence of LEV. **C** Sliced side view with electrostatic surface charge and bound LEV (yellow). The boxed region is enlarged in the right panel. **D** Cryo-EM density map of bound LEV (green) and the coordinating residues of SV2A (blue) as sticks. The density-modified (Phenix) map is contoured at 0.95σ in ChimeraX. **E** Detailed view of the LEV (green) interacting residues in SV2A. Polar interactions are shown as black dashed lines. Distances of π–π interactions or other hydrophobic interactions are indicated along solid black lines in Å. The right panel shows a rotated view from a different angle.

Fig. 13E). For larger molecules like Padsevonil (another tightly binding racetam), the di-tyrosine motif could occlude the path to extracellular substantially[60]. LEV is bound to SV2A through multiple interactions, most obvious by sandwiching (π-π interaction) between the conserved Trp-residues 300 and 666 (Fig. 5E). The oxo-group of the pyrrolidone-ring of LEV forms a hydrogen bond with Tyr462, and the branched butyl-amide moiety of LEV is positioned between TM-helices 4,5,7 and 10. From our density, we propose that the ethyl-group of this moiety points towards TM helix 4 and interacts with Ile273 through a hydrophobic interaction. In SV2B, that binds very weakly to LEV with a Ki of ~1mM[60], the Ile273 position is occupied by leucine (Supplementary Fig. 12). While LEV fits snuggly into the pocket with an isoleucine at this position, a leucine like in SV2B could clash with the compound. The amide of the butyl-amide points towards Asp670 on TM helix 7 and Cys297 on TM helix 5 (Fig. 5E). The NH_2-group is coordinated by the carboxy-group of Asp670 (~2 Å distance) and the oxygen of the butyl-amide could interact with Cys297 through a hydrogen bond (2.5 Å distance) (Fig. 5E). The corresponding residue of Cys297 is a glycine in human, mouse or sheep SV2B (Supplementary Fig. 12) and would thus not contribute to the coordination of LEV, a difference that could explain the very weak binding of LEV to SV2B. Additionally, Asn667, Ile663 and Lys694 of which mutations have been reported to impair binding to LEV[23], are in very close vicinity. Brivaracetam (BRV), a more potently binding racetam differs from LEV by an additional hydrophobic element, a propyl group, attached to the pyrrolidone-ring (Fig. 5A). The propyl-group could mediate interactions within a hydrophobic patch that is formed by Ile663 and Val608 and the aromatic ring of Tyr461 which would explain its stronger binding and which has been characterized in a recent structure by Yamagata et al.[52]. From our analysis we could not find an obvious explanation why SV2C is not binding to LEV[21] because all relevant residues for LEV binding in SV2A and SV2C are identical.

Discussion

The SV2 family of proteins, discovered more than 30 years ago has remained enigmatic with respect to many aspects of its function. However, SV2 proteins turned out to be medically of high relevance despite their unclear role in neurotransmission. They were unveiled as the protein receptors of many different serotypes of botulinum neurotoxins and proposed, but also questioned, to represent the receptor for tetanus neurotoxin in central neurons. Remarkably, a major drug against epilepsy – Levetiracetam - discovered in the 1970s by UCB /Belgium turned out to bind to SV2A. Other than one might assume, the compound did not immediately uncover more of SV2's secrets, however it would remain an important tool on the way to a deeper understanding of SV2 proteins besides its medical use.

Structural studies on CNT-SV2-interactions have been conducted largely with isolated SV2C-LD4 or SV2C-SV2A LD4 chimeras, which provides us only with a limited window for probing these important interactions. To gain more insights into the molecular details of SV2 proteins and their interactions with toxins and anti-epileptic drugs, experimental structures are needed, ideally using full-length SV2 protein.

Our study revealed that TeNT binds to the N-terminal end of the LD4 domain of SV2A in parallel orientation, a surprising finding which has not been anticipated earlier and which is unique for CNTs to date. The structure corroborates earlier data that showed a binding of TeNT to SV2 proteins[38] and provides strong support for their role as TeNT protein-receptors in central neurons. Further, the conflicting finding that TeNT and BoNT/A H_C domains do not compete for SV2 binding[39] can be readily explained from the revealed binding site of TeNT on the opposite end of the LD4, which could apparently have both toxin H_C domains bound at the same time. The interface between SV2A and TeNT-H_C, as concluded from the comparison of LD4 crystal structures and our cryo-EM structure, could only be formed with full-length SV2A due to the completeness of the N-terminal end of the LD4 β-helix. This points to potential limitations to use isolated LD4 in capturing the diversity of CNT interactions. Moreover, we could reveal the binding of the lipidic ganglioside receptors of TeNT-H_C while being bound to SV2A, visualizing, and reinforcing the principles of the decades-old theory of dual-receptor recognition for neuronal toxin entry[61]. We cannot answer whether the co-purification of endogenous

gangliosides is due to interactions with SV2A as we do not see clear density proximal to SV2A that could stem from ceramide moieties. But it could be that gangliosides are enriched in the proximity of SV2A. Gangliosides have been shown to be associated with Syts[62], hence SV2 proteins and Syts could form ganglioside rich patches that recruit CNTs with higher probability. The importance of simultaneously bound ganglioside- and SV2A-receptors is also reflected in the adaption of the angle of the LD4-binding β-hairpin relative to the rest of the toxin-H_C to fulfill both conditions optimally (Supplementary Fig. 8). Through this, the chance for endocytosis into SVs at extremely low concentrations of the toxin would be greatly enhanced. We further suggest why SV2C is not bound by TeNT as the N-terminus of the SV2C-LD4 deviates from SV2A and SV2B, however this requires insight into experimental structural data on SV2C for verification. Presumably, the inability to bind SV2C would ensure that TeNT is only rarely entering recycling SVs of motor neurons (mainly SV2C) but does so with great efficacy only after reaching central neurons (mainly SV2A) by retrograde transport as part of the toxin's strategy to reach the type of neurons where the light chain exerts its strongest effect.

Additionally, the revealed binding site for TeNT has implications for medical and biotechnological applications of CNTs. CNTs (mainly BoNT/A serotypes) are utilized in the treatment of spasms and chronic pain apart from their cosmetic uses. Immune responses can arise due to repeated application of the toxins, which could be overcome by higher potencies of the toxin. From our structure it could be concluded that one could generate toxin preparations (containing two populations) which target both ends of an SV2 LD4 to increase the potency and reducing the amount of required toxin. For instance, chimaeras of TeNT and BoNT have already been generated, in support of the general feasibility of this approach[63]. CNTs have also been engineered for targeted delivery of different proteins to neurons, by exchanging the light chain with a different cargo[64–66] or introducing proteases with different substrate specificities[67]. Future engineering approaches with the H_C of CNTs will shed light on the possibility to employ the TeNT binding site for the abovementioned uses.

The MFS architecture of SV2 proteins has not been challenged in general, but due to the unclear function, structural insights as provided in our study reinforce the concept of a membrane transporter. The outward-open conformation with a clear cavity between the N- and C-terminal halves of the protein resembles other MFS transporters (e.g URAT1, Supplementary Fig. 13). The presumed substrate pocket, as delineated by the bound LEV molecule in the center of the membrane plane is built from highly conserved amino acids in support of their functional significance. Two tryptophan residues that sandwich also the planar LEV molecule have been shown to be essential in rescue experiments, but it remains to be seen if and which solute they would probably bind. The pocket is further featuring several polar residues in the vicinity of the central area between Trp300 and Trp666 suggesting an interaction with a substance that has at least polar elements. Recently, it was shown that SV2A would transport galactose when expressed in yeast cells[7]. A hexose could indeed fit into the pocket and interactions with Trp-sidechains are common in carbohydrate interactions. Whether this or other sugars are transported substances, needs to be tested in SVs though. Although the function of the LD4 is currently unclear and make SV2 unique among MFS transporters, its connection to more than two TM-helices (through the disulfide bond) that are involved in LEV binding suggest that it is either mechanistically involved in a transport cycle or of regulatory function e.g. through binding of yet unknown modulators. Whether the uncapped architecture of the β-strands on the LD4 termini is part of their intrinsic function in SV2 proteins and thus constitutes an Achille's heel that is consequently targeted by CNTs will only become clear when we understand more about this domain.

The binding of LEV as observed in our structures is largely in line with earlier binding studies using radiolabelled racetams[23]. These binding studies together with our structure further show that the core elements of binding in racetams are the pyrrolidone-ring and the butyl-amide group, and that the latter confers specificity for SV2A. The butyl-amide moiety branches into two groups, the amide and the ethyl-group which appear rather similar at the resolution in our maps although one arm of our density appears slightly bi-lobed which is more consistent with the amide group (Supplementary Fig. 11A). We reconstructed the most plausible rotamer by taking the best match to the observed density, the chemistry of the side chains, the physical characteristics of groups on LEV and differences to the SV2B isoform into account. Based on our obtained density the ethyl-group fits better when pointing towards Ile273 than towards Cys297. If the ethyl-group was pointing towards Cys297, it would be facing a glycine in SV2B. A glycine residue would not be prohibitive for an ethyl-group in this space and thus not explain very well that SV2B binds only very weakly to LEV but suggests instead that a critical interaction is missing. From our density, the amide of LEV is positioned such that the oxygen interacts with Cys297 and the NH_2-group with Asp670. In SV2B, the interaction would be limited to Asp670 through the NH_2-group. We thus suggest that Cys297 is a critical residue underlying LEV's discrimination of SV2A over SV2B, together with Ile273 the only residue that differs in the binding pocket of the two isoforms. During the revision of this study, another team has investigated the binding of LEV to a mutated SV2B protein[60]. When Gly240 was mutated to cysteine in hSV2B (the equivalent residue is Cys297 in SV2A), the K_i of LEV increased from ~1 mM to 13 μM, a nearly hundredfold increase, similar to wild-type hSV2A (4.4 μM). This phenotype is in line with a hydrophilic interaction of LEV and Cys297 in SV2A and this fits also best to our density, but a hydrophobic interaction of Cys297 with the ethyl moiety can also not be excluded by us with certainty. Recently, other research groups have provided structures of SV2 proteins bound to racetams[52,60]. We note that in the study of Yamagata et al. the LEV molecule was placed differently from our study with respect to the rotamer of the butyl-amide as the authors placed the ethyl-group pointing to Cys297[52] which would reflect a hydrophobic interaction. Mutating this residue to residues with hydrophobic character (e.g. Cys297Val) or hydrophilic character (Cys297Ser) could shed light on the nature of interactions in this region together with structures of much higher resolution and different LEV derivatives. While our data provides an explanation for the lack of LEV binding in SV2B, we note that this is not obvious for SV2C because all LEV-interacting residues are identical. Hence, differences outside of the binding pocket must account for the discrimination of LEV in SV2C. Alternatively, a different preferred conformation of SV2C could also contribute to the much lower LEV binding. The structure of SV2A bound to LEV presented herein opens possibilities for the development of even more potent molecules on a rational basis.

The structure of SV2A from Yamagata et al. (also in the presence of LEV) aligns globally very well with ours (Supplementary Fig. 13A) and the authors also consider their structure as outward-open. Related transporters have been captured in the (outward)-occluded state which is characterized by constriction of the passage to the substrate pocket by TM helix 7[68], supporting that the observed conformational state in our SV2A structure and the one of Yamagata et al. is outward-open (Supplementary Fig. 13B, C). Further, the position of the di-tyrosine motif (Y461, Y462), another shared feature with related MFS transporters is closer to the one seen in outward-open conformation[68] (Supplementary Fig. 13D). Interestingly, the SV2A-structure of Mittal et al. (bound to a close derivative of Padsevonil) seems to be in an outward-occluded state, which was also noted by the authors. Interestingly, the occluded state appears to found on a movement of helix 1 towards the central cavity, and not by helix 7 as seen in the occluded state of URAT1 (Supplementary Fig. 13B, C). Definite answers will require the capture of other states and intermediates of SV2A.

Furthermore, recently published SV2A and SV2B structures[52,60,69] differ from our structures with respect to the disulfide-bridge between Cys198 and Cys583 (SV2A numbering) that we can clearly resolve in our maps but that is not clear in other published maps and that was consequently not built in the model[52,60,69]. Whether this bond is only formed in neuronal cells is difficult to resolve at the moment. It could also be that a lower local resolution in the other maps compared to our maps prevents the visibility of the disulfide bridge or that this bond is dynamically forming and breaking. The disulfide bridge could have impact for the mobility of the LD4 and functional implications.

In summary, our work provides a structural basis for the further characterization of SV2 proteins, based on natively purified protein. We could reveal the precise location of the LEV binding pocket which appears to coincide with a substrate pocket of a yet unknown substance. The dimensions and chemistry of this pocket will be aiding in limiting substrate searches and future developments for improved SV2A-targeting drugs will benefit from structure-based drug design through the presented data. Further, our structure of a ternary complex composed of SV2A, endogenous gangliosides and the H_C of TeNT, together with older functional data[38] provides compelling evidence for SV2A as the long-sought-after receptor of TeNT in central neurons. The unexpected binding mode and simultaneous binding to lipids expands our knowledge on CNT binding to its receptors, settles open controversies for TeNT and opens up interesting possibilities for toxin engineering to address neuronal cargo delivery and improving therapeutic applications of CNTs.

Methods

Ethical statement

We confirm that our research complies with all relevant ethical regulations. The project involved the generation of camelid antibodies for which llamas were immunized, and blood samples were collected in compliance with both the European legislation (EU directive 2010/63/EC) and the Belgian Royal Decree of 29 May 2013 concerning the protection of laboratory animals with the exception that the animals are not specifically bred for such use. The llamas were housed in a center (farm), which is licensed by the Belgian competent authorities (accreditation number LA 1700601) and all staff involved was appropriately trained. The immunization and blood collection of the llamas has been approved by the authorized local Animal Ethics Review board with reference number 12-xxx-1.

Expression constructs and nanobody sequences

PMbs were generated as described previously[49,70,71] but with a C-terminal twin-strep-tag II (TSII) that was inserted into the C-terminal MBP by PCR. Briefly, Nb1-5 were PCR amplified and sub-cloned into the vector pBXNPHM3[70] (Addgene #11099) and fused with a C-terminal (TSII-tagged) MBP that lacks the first six amino acids (starting at Lys7) through a di-Pro linker. The resulting expression construct contains from N- to C-terminus: a pelB leader sequence, a deca-Histidine tag, an MBP, a 3C cleavage site, a Nb, the proline-proline linker, and the truncated MBP followed by a TSII, as depicted in Supplementary Fig. 1A.

BoNT/A1-H_C, corresponding to residues 871–1296 of the holotoxin, was synthesized (Twist biosciences) in three fragments that were fused by typeIIS restriction enzyme cloning with *SapI*. The expression construct was subcloned into a peT28a vector using *NcoI* (encoding the start methionin) and *NotI* (Stop codon 5′ of *NotI*). The construct encodes for an N-terminal deca-Histidine tag followed by a 3C cleavage site followed by BoNT/A1-H_C. Between the 3C-site and BoNT/A1-H_C the construct contained a *BamHI* restriction site to insert other H_C-domains using *BamHI* and *NotI*. For the expression of TeNT-H_C, the H_C-domain of TeNT encoding the C-terminus of the toxin from Glu875 to Asp1315 was amplified from the plasmid pKS1 (pKS1 was a gift from Neil Fairweather (Addgene plasmid # 84079[72]) with flanking *BamHI* and *NotI* sites including a stop codon 5′ of *NotI* and exchanged for BoNT/A1-H_C in the peT28a vector digested with *BamHI* and *NotI* resulting in a N-terminally deca-Histidine-tagged expression construct.

Amino acid sequences of the nanobodies for purification and cryo-EM (PMb linker underlined and in italics):

Nb1 (PMb1):

QVQLVESGGGSVQPGGSLRLSCAVSGTIFSINGMGWYRQAPGKQ-RELVAYITSGGTTSYVDFVAGRFTISRDNTKNTVYLQMNSLKPEDTA-VYFCNVARNWGLEPFGSWGQGTQVTV*PP*

Nb2 (identical to Nb-8783 used by Mittal et al.[60]) (PMb2):

QVQLVESGGGLVQPGGSLRLSCAASGSIFNMRVMGWYRQAPGEQ-RESVASMASGDKTTYADSVKGRFTISRDNAKNTVALQMNSLKPEDTA-VYYCHAVDLTRNGPRVYWGQGTQVTV*PP*

Nb5 (PMb5):

QVQLVESGGGLVQAGGSLRLSCAASGRTFSRFIMGWFRQAPGKER-EFVAAVGKSGDTTYYADSMSGRFAISRDNAKNTVYLQMISLKPEDTAVYY-CAADSSYFYHTHESEYDYWGQGTQVTV*PP*

Truncated MBP for PMbs fused to Nbs after PP-linker with C-terminal twin-StrepTag:

LVIWINGDKGYNGLAEVGKKFEKDTGIKVTVEHPDKLEEKFPQVAA TGDGPDIIFWAHDRFGGYAQSGLLAEITPDKAFQDKLYPFTWDAVRYN GKLIAYPIAVEALSLIYNKDLLPNPPKTWEEIPALDKELKAKGKSALMFNL QEPYFTWPLIAADGGYAFKYENGKYDIKDVGVDNAGAKAGLTFLVDLIK NKHMNADTDYSIAEAAFNKGETAMTINGPWAWSNIDTSKVNYGVTVLPT FKGQPSKPFVGVLSAGINAASPNKELAKEFLENYLLTDEGLEAVNKDKPL GAVALKSYEEELAKDPRIAATMENAQKGEIMPNIPQMSAFWYAVRTAVIN AASGRQTVDEALKDAQTPGSGGGSAWSHPQFEKGGGSGGGSGG-SAWSHPQFEKAA

Nanobody selection

SV2A nanobodies (Nbs) were identified from two immunized llamas (*Lama glama*) following a prime-boost vaccination schedule. Immunizations were executed at a contract research organization meeting European animal welfare legislation and following approval by an ethical committee. Humoral seroconversion to human SV2A was primed by genetic vaccination applying four 2 mg doses of full-length human SV2A DNA cloned in pCDNA3.1(+). DNA was administered with intervals of two weeks following an in vivo electroporation protocol[73]. Llamas were additionally boosted four times with membrane extracts derived from human SV2A expressed in HEK293 cells again with two-week intervals. Each dose corresponded to 2-4 mg of total protein. The in vivo matured nanobody repertoires were cloned in a dual-purpose phagemid vector allowing phage display and expression of soluble nanobody as C-terminally His6-c-Myc tagged protein[74]. Recombinant Flag-tagged rat SV2A protein (kindly provided by UCB Pharma, Belgium) was used for in solution panning continuously in the presence of 100 μg/ml of Levetiracetam according to standard methods[74]. Following two rounds of biopanning, phage outputs were infected in *Escherichia coli* TG1 and single colonies carrying monoclonal nanobodies were cultured in 96-well plates to prepare periplasmic extracts[74] for downstream specificity assessment. Nb specificity was assessed by ELISA in the presence of excess amounts of Levetiracetam. Binding of periplasmic extracts harboring c-Myc-tagged nbs to Flag tag-captured detergent soluble rat SV2A was detected with an anti c-Myc-horseradish peroxidase detection antibody conjugate (Roche). Three SV2A-specific Nbs belonging to different complementarity-determining region 3 (CDR3) sequence clusters (Nb1, Nb2 and Nb5) were retained for further use as structural biology chaperone.

Protein expression and purification

PMbs were expressed and purified as described earlier[49,70,71]. Briefly, MC1061 bacteria were transformed with pBXNPHM3-PMb1-5, grown at 37 °C in terrific broth (TB) with 100 μg/ml ampicillin until an OD_{600} of 1.2 was reached and subsequently induced with 0.024% L-arabinose. Expression was performed for 3.5 h at 37 °C. Cells were harvested by

centrifugation and the resulting pellet was resuspended in 50 mM Tris-HCl pH 8, 150 mM NaCl, 0.5 mM EDTA, 10% glycerol containing protease inhibitors (Roche, cOmplete, EDTA-free Protease Inhibitor Cocktail) and frozen at −30 °C for later use. BoNT/A1- and TeNT-H_Cs were expressed in the same way as described for PMbs, but instead BL21-DE3 cells were transformed with the respective peT28a expression vectors under selection of 50 μg/ml kanamycin and IPTG was applied at a concentration of 0.5 mM to induce protein expression at an OD_{600} of 0.6. The cells expressing BoNT/A1-H_C and TeNT-H_C were harvested by centrifugation and the respective pellets were frozen in a buffer containing 50 mM Tris-HCl pH 8, 150 mM NaCl, 0.5 mM EDTA, 10% glycerol and protease inhibitors and stored at −30 °C.

For the purification of PMbs, frozen pellets were thawed, additional protease inhibitors were added, and the cells were incubated with lysozyme for 30 min at RT under stirring. All subsequent steps were performed at 4–8 °C. Subsequently, DNase I at 50 μg/ml and $MgSO_4$ (5 mM final concentration) were added, and cells were lysed by sonication. Cell debris was removed by ultracentrifugation in a 45Ti rotor (Beckman) at 130,000 g_{av} for 30 min. The resulting supernatant was applied to NiNTA-resin in batch for 1.5 h, washed with 150 mM NaCl, 40 mM imidazole pH 7.6, 10% glycerol and bound proteins were eluted using 150 mM NaCl, 300 mM imidazole pH 7.6 and 10% glycerol. An overnight cleavage using HRV 3C protease was performed during dialysis against 150 mM NaCl, 10 mM Hepes-NaOH, 20 mM imidazole, pH 7.6, 10% glycerol. The purification tag (N-terminal deca-His-MBP) was removed by re-binding to NiNTA resin and the flow-through containing PMbs was concentrated and subjected to gel filtration chromatography on a Superdex 200 pg 16/600 column (Cytiva) which was previously equilibrated with 150 mM NaCl, 10 mM Hepes-NaOH 7.6. Peak fractions were pooled, supplemented with 10% glycerol, aliquoted, frozen in liquid nitrogen and stored at −80 °C.

BoNT/A1- and TeNT- H_Cs were purified in similar manner with the exception that eluted proteins at a concentration of 11 and 17 mg/ml for BoNT/A1-H_C and TeNT- H_C, respectively, were dialyzed against 200 mM NaCl, 20 mM Hepes-NaOH pH 7.6, 10% glycerol without cleaving off purification tags by 3C protease cleavage. The dialyzed proteins at 11 and 17 mg/ml for BoNT/A1-H_C and TeNT-H_C were frozen using liquid Nitrogen and stored at −80 °C and tested for monodispersity by injection into an HPLC on a Superdex 200 Increase 5/150 column before mixing with SV2A.

SVA purification from sheep brain

Lamb brains (*Ovis aries*) were obtained from freshly slaughtered animals at the Abattoir of Brussels (Ropsy Chaudronstraat 24, 1070 Brussels, Belgium), where lambs are slaughtered 2 days/week for human consumption, through an appointment with the veterinarians. The brains were immediately placed on ice and kept cool during transport back to the laboratory where they were immediately processed. Sheep brains were roughly cleaned from larger blood vessels, excess connective tissue and bone pieces, cut into ~2 cm blocks, frozen in liquid nitrogen and stored at −80 °C until use. The brains were cut such that all parts of the brain were included in a round of purification (e.g. ½ brain including cortex and cerebellum) to avoid variations across different purifications in the yield of SV2A. For a typical purification, a total of two brains (~180 g) were homogenized with a glass-Teflon homogenizer in 50 mM Hepes pH 7.6, 250 mM NaCl, 10% glycerol and protease inhibitors (Roche, cOmplete, EDTA-free Protease Inhibitor Cocktail). Subsequently, membranes were solubilized and proteins extracted by addition of (final concentrations 2% n-Dodecyl-β-D-Maltopyranoside (DDM) and 0.2 % cholesteryl-hemisuccinate (CHS) for two hours at 4 °C under constant stirring. The crude lysate was centrifuged at 130,000 g_{av} in a 45Ti rotor (Beckman) for 45 min to remove insoluble parts. The supernatant was incubated in batch with streptactin resin (IBA, Göttingen) which was pre-loaded with ~2 mg purified TS-II tagged SV2A-specific PMbs. After an incubation time of 2 h unbound proteins were washed away with a buffer containing 30 mM Hepes-Na pH 7.6, 150 mM NaCl, 2.5 mM maltose, 10% glycerol, 0.03% DDM and 0.006% CHS and subsequently eluted with the same buffer containing additionally 10 mM biotin. The eluate was concentrated to 6 mg/ml and frozen in liquid nitrogen for later use in differential scanning fluorometry, mass spectrometry or cryo-EM experiments. When we used the membranes of a S1 fraction through subcellular fractionation, removing already substantial amounts of plasma, cytosol and mitochondria, we had slightly lower yields and SV2A preparations of comparable purity. The purification from whole-brain homogenate was therefore chosen as the standard.

Expression and purification of VGLUT1

Rat VGLUT1 that was used as a control for thermal unfolding experiments was expressed in tsA201 cells by transient transfection and purified as described earlier[75,76].

Western blotting

For the evaluation of SV2A specificity of the Nbs, crude mouse brain homogenate (1 brain in 6 ml) was lysed in 200 mM NaCl, 25 mM Hepes-Na, pH 7.6, 10% glycerol and 2% DDM, 0.4 % CHS for 1 h at 4 °C. The soluble supernatants, after centrifugation for 1 h at 13,000 × *g* in a cooled benchtop centrifuge, were applied to 30 μl (bed volume) of streptactin beads (IBA, Göttingen, Germany) pre-loaded with the respective tagged PMbs. After washing four times with 1 ml of 150 mM NaCl, 20 mM Hepes-Na, pH 7.6, 10% glycerol, 0.03% DDM, 0.006 CHS, in a 1.5 ml tube, PMbs with bound antigens were eluted in 80 μl of the wash buffer supplemented with 10 mM biotin. Equal volumes of input material and eluate were loaded on SDS-PAGE gels and transferred on PVDF membranes by semi-dry western blotting. The blots were probed with isoform-specific affinity-purified rabbit antibodies (all from Synaptic Systems, Göttingen, Germany) to SV2A (Cat. Nr. 119003), SV2B (Cat. Nr. 119103) and SV2C (Cat. Nr. 119203) and developed with HRP-conjugated goat-anti-rabbit secondary antibodies in a BioRad ChemiDoc imager by chemiluminescence.

Thermal shift assay/differential scanning fluorimetry (DSF)

Protein stability was assessed by means of thermal unfolding, carried out through a temperature ramp using a real-time PCR cycler (CFX connect, Bio-Rad) following previously published protocols[77]. In this assay, initially buried cysteines become accessible through thermal unfolding and react with the CPM fluorophore (7-Diethylamino-3-(4′-Maleimidylphenyl)-4-Methylcoumarin), which creates fluorescent adducts. CPM dye at 5 mg/ml in DMSO was diluted to 0.1 mg/ml with assay buffer (10 mM Hepes-NaOH pH 7.5, 150 mM NaCl, 0.03% DDM) and incubated in the dark under mild agitation for one hour at RT.

For each thermal shift assay experiment 2–3 μg of SV2A-PMb5 or rVGLUT1 bound to a PMb (generated from anti-VGLUT1/2-Nbs[76]) were diluted in assay buffer and mixed with either LEV at 250 μM or assay buffer in a total volume of 20 μl. CPM equilibrated in assay buffer was added to a final concentration of 0.02 mg/ml and incubated for 10 min before applying the temperature ramp in the PCR cycler. After an initial incubation of 90 s at 18 °C, the temperature was raised by 1 °C per 12 s until a temperature of 90 °C was reached. The fluorescence change was monitored using a filterset for FAM fluorescence (470 nm excitation, 520 nm emission). Unfolding spectra were analyzed using the CFX Maestro software, and the melting temperature Tm was extracted from the inflection point of the unfolding curves. ΔTm was calculated as the difference of melting temperatures in the presence and absence of LEV. For each condition three replicates were performed and standard deviations are indicated for the unfolding curves. The PMbs are

devoid of free cysteines and remain undetected in the assay with CPM dye.

Cryo-EM sample preparation and data collection

The SV2A-PMb5 complex at a concentration of 6 mg/ml was mixed in a 1:2 molar ratio with TeNT-H_C (or BoNT/A1-H_C). Prior to complex formation SV2A-PMb5 was separately incubated with 2.5 mM maltose to restrict movements in the MBP moiety of PMb5, and TeNT-H_C was mixed with 0.03 % DDM and 0.006% CHS. After an incubation time of 1 h on ice, the mixture was subjected to size exclusion chromatography using a Superdex 200 Increase 5/150 column (Cytiva) on an HPLC that was equilibrated with a buffer containing 10 mM Hepes pH 7.5, 150 mM NaCl, 0.03% DDM and 0.006% CHS. The peak fraction was concentrated to 7 mg/ml and used immediately in cryo-plunging experiments. 3ul of the complex were subsequently applied to glow-discharged holey grids (Quantifoil R1.2/1.3 Cu 300 mesh) and plunged into liquid ethane after a blotting time of 2 s at 90% humidity using a CP3 plunger (Gatan). For the LEV dataset, 30 min before cryo-plunging, the tripartite complex was incubated with LEV at a final concentration of 250 μM. SV2A in complex with the different PMbs were prepared for plunging in similar manner.

Movies were collected on a JEOL cryoARM300 microscope with 300 kV accelerating voltage and equipped with a K3 direct electron detector (Gatan) and energy filter with 20 eV slit. 60 frames per movie were collected in automatic manner using SerialEM 4.1.0 beta26[78] at an exposure time of 2.796 s, total dose of about 60 e^-/Å2 and a defocus of 0.8-2.5 μm using a 3 × 3 multi-shot pattern. Movies were acquired at a nominal magnification of 60'000 and a pixel size of 0.71Å. A total of 22295 and 17809 movies were collected for the SV2A-TeNT-H_C-PMb5 complex and LEV-SV2A-TeNT-H_C-PMb5 datasets, respectively.

Processing of cryo-EM data

The movies were pre-processed in CryoSPARC Live for motion correction using Patch Motion correction and the contrast transfer function (CTF) of the motion-corrected images was estimated using CryoSPARC CTF estimation[79]. All subsequent steps were done in cryoSPARC-v.4[79]. For both datasets, initially a similar approach of processing was chosen. The particles were picked using a multi-picking approach (blob, topaz, template picker) and subjected to several rounds of 2D classification. Templates were generated from a small subset from blob picking for use as input during template picking. For the tripartite complex consisting of SV2A-TeNT-H_C-PMb5, the selected particle stack after 2D classification was cleaned from duplicates and applied to multiple rounds of heterogeneous refinement using five ab-initio maps as initial input. A non-uniform refinement was done with a stack of particles from multiple good lines of heterogeneous refinement. The resulting particle stack was then subjected to a 3D classification into two classes with a focused mask on the TM part. Next, duplicates were removed and the resulting stack was further processed in a non-uniform refinement. A reference-based motion correction step was conducted and the polished particles were further used in a CTF refinement. A final non-uniform refinement provided a map of 3.25Å which was subsequently sharpened using DeepEMhancer[80].

For the LEV dataset, after several rounds of 2D classification, the particles were further cleaned by multiple rounds of heterogeneous refinements in two processing lines using four and five ab initio maps, respectively. Particles from good heterogeneous refinements were combined, followed by a removal of duplicates and a non-uniform refinement that yielded a map at 3.60Å. The map was additionally processed using a Local refinement with a small mask at the position of LEV which improved the resolution to 3.35 Å and was further density optimized in Phenix. Throughout all processing no symmetry (C1) was applied.

Atomic model building

DeepEMhancer and Phenix-density modified maps were used for model building and for the preparation of figures. An Alphafold2[56] model was generated for the sequences of sheep SV2A (Uniprot entry A0A836APF1) and Nb5. PDB entry 1FV2 (H_C fragment of tetanus toxin)[42] was used for model building of TeNT-H_C. The models were rigid-body fitted to the experimental cryo-EM map of SV2A-TeNT-H_C-PMb5. Stretches in the models that were not visible in the map were removed. The SV2A-TeNT-H_C-PMb5 model was built first and served as starting point for building the LEV-SV2A-TeNT-H_C-PMb5 model. The models were subjected to iterative rounds of Phenix refinement (Phenix v.1.21.1-5207[81]) and manual model building in Coot 0.8.9.2[82]. For SV2A-TeNT-H_C-PMb5 all residues could be modeled except for the N-terminus (1–144), and residues 322-329 and 401-420 in SV2A, residues 983-987 and 1182-1187 in TeNT-H_C and the MBP moiety of PMb5. Lower resolution regions in SV2A such as H2 and H3 were modeled from the Alphafold2 prediction. Pymol v.2.0.7 and v.2.5.4, and ChimeraX-1.3[83] were used for the illustration of the structures and maps.

Reporting summary

Further information on research design is available in the Nature Portfolio Reporting Summary linked to this article.

Data availability

Atomic models have been deposited in the Protein Data Bank (PDB), and cryo-EM maps and corresponding half maps and masks can be accessed through the Electron Microscopy Data Bank (EMDB). The atomic models have been deposited under accession code 9FYQ (SV2A-PMb5-TeNT-H_C) and 9FYR (LEV-SV2A-PMb5-TeNT-H_C). The corresponding maps can be found under EMD-50889 (global map SV2A-PMb5-TeNT-H_C), EMD-50890 (local map 'TeNT-Gangliosides') and EMD-50891 (LEV-bound SV2A-PMb5-TeNT-H_C). The source data underlying Supplementary Figs. 1C–E, 4A, B, 9 are provided as a Source Data file. Previously published structures used in a comparative analysis in this manuscript can be found with the following PDB codes: 8JLG (cryo-EM structure of SV2A-BoNT/A2-Hc), 8JLC (cryo-EM structure of SV2A-BoNT/A2-Hc with LEV), 8UO9 (cryo-EM structure of SV2A with a Nanobody), 9B1L (Urate bound human URAT1 in the outward-facing state), 9B1K (Urate bound human URAT1 in the occluded state). 5N0B (crystal structure of TeNT-RBD), 5MOY (crystal structure BoNT/A2-RBD with SV2A-LD4), 6ES1 (crystal structure BoNT/A2-RBD with SV2A-LD4), 7UIA (crystal structure BoNT/E-RBD with SV2A-LD4), 5JLV (crystal structure BoNT/A-RBD with SV2C-LD4), 7Z5T (crystal structure BoNT/A2-RBD), 1FV2 (crystal structure TeNT-RBD). Source data are provided with this paper.

References

1. Takamori, S. et al. Molecular anatomy of a trafficking organelle. *Cell* **127**, 831–846 (2006).
2. Ciruelas, K., Marcotulli, D. & Bajjalieh, S. M. Synaptic vesicle protein 2: a multi-faceted regulator of secretion. *Semin. Cell Dev. Biol.* **95**, 130–141 (2019).
3. Bartholome, O. et al. Puzzling out synaptic vesicle 2 family members functions. *Front. Mol. Neurosci.* **10** https://doi.org/10.3389/fnmol.2017.00148 (2017).
4. Feany, M. B., Lee, S., Edwards, R. H. & Buckley, K. M. The synaptic vesicle protein SV2 is a novel type of transmembrane transporter. *Cell* **70**, 861–867 (1992).
5. Bajjalieh, S. M., Peterson, K., Shinghal, R. & Scheller, R. H. SV2, a brain synaptic vesicle protein homologous to bacterial transporters. *Science* **257**, 1271–1273 (1992).
6. Janz, R., Goda, Y., Geppert, M., Missler, M. & Südhof, T. C. SV2A and SV2B function as redundant Ca2+ regulators in neurotransmitter release. *Neuron* **24**, 1003–1016 (1999).

7. Madeo, M., Kovács, A. D. & Pearce, D. A. The human synaptic vesicle protein, SV2A, functions as a galactose transporter in Saccharomyces cerevisiae. *J. Biol. Chem.* **289**, 33066–33071 (2014).
8. Ono, Y., Mori, Y., Egashira, Y., Sumiyama, K. & Takamori, S. Expression of plasma membrane calcium ATPases confers Ca(2+)/H(+) exchange in rodent synaptic vesicles. *Sci. Rep.* **9**, 4289 (2019).
9. Crowder, K. M. et al. Abnormal neurotransmission in mice lacking synaptic vesicle protein 2A (SV2A). *Proc. Natl Acad. Sci. USA* **96**, 15268–15273 (1999).
10. Chang, W. P. & Südhof, T. C. SV2 renders primed synaptic vesicles competent for Ca2+ -induced exocytosis. *J. Neurosci.* **29**, 883–897 (2009).
11. Nowack, A., Yao, J., Custer, K. L. & Bajjalieh, S. M. SV2 regulates neurotransmitter release via multiple mechanisms. *Am. J. Physiol. Cell Physiol.* **299**, C960–C967 (2010).
12. Drew, D., North, R. A., Nagarathinam, K. & Tanabe, M. Structures and General Transport Mechanisms by the Major Facilitator Superfamily (MFS). *Chem. Rev.* **121**, 5289–5335 (2021).
13. Schivell, A. E., Batchelor, R. H. & Bajjalieh, S. M. Isoform-specific, calcium-regulated interaction of the synaptic vesicle proteins SV2 and synaptotagmin. *J. Biol. Chem.* **271**, 27770–27775 (1996).
14. Schivell, A. E., Mochida, S., Kensel-Hammes, P., Custer, K. L. & Bajjalieh, S. M. SV2A and SV2C contain a unique synaptotagmin-binding site. *Mol. Cell Neurosci.* **29**, 56–64 (2005).
15. Pyle, R. A., Schivell, A. E., Hidaka, H. & Bajjalieh, S. M. Phosphorylation of synaptic vesicle protein 2 modulates binding to synaptotagmin. *J. Biol. Chem.* **275**, 17195–17200 (2000).
16. Yao, J., Nowack, A., Kensel-Hammes, P., Gardner, R. G. & Bajjalieh, S. M. Cotrafficking of SV2 and synaptotagmin at the synapse. *J. Neurosci.* **30**, 5569–5578 (2010).
17. Zhang, N. et al. Phosphorylation of synaptic vesicle protein 2A at Thr84 by casein kinase 1 family kinases controls the specific retrieval of synaptotagmin-1. *J. Neurosci.* **35**, 2492–2507 (2015).
18. Harper, C. B. et al. An epilepsy-associated SV2A mutation disrupts synaptotagmin-1 expression and activity-dependent trafficking. *J. Neurosci.* **40**, 4586–4595 (2020).
19. Carlson, S. S. SV2proteoglycan: a potential synaptic vesicle transporter and nerve terminal extracellular matrix receptor. *Perspect. Dev. Neurobiol.* **3**, 373–386 (1996).
20. Bradberry, M. M., Peters-Clarke, T. M., Shishkova, E., Chapman, E. R. & Coon, J. J. N-glycoproteomics of brain synapses and synaptic vesicles. *Cell Rep.* **42**, 112368 (2023).
21. Lynch, B. A. et al. The synaptic vesicle protein SV2A is the binding site for the antiepileptic drug levetiracetam. *Proc. Natl Acad. Sci.* **101**, 9861–9866 (2004).
22. Löscher, W., Gillard, M., Sands, Z. A., Kaminski, R. M. & Klitgaard, H. Synaptic vesicle glycoprotein 2A ligands in the treatment of epilepsy and beyond. *CNS Drugs* **30**, 1055–1077 (2016).
23. Shi, J. et al. Combining modelling and mutagenesis studies of synaptic vesicle protein 2A to identify a series of residues involved in racetam binding. *Biochem Soc. Trans.* **39**, 1341–1347 (2011).
24. Lee, J. et al. Exploring the interaction of SV2A with racetams using homology modelling, molecular dynamics and site-directed mutagenesis. *PLoS ONE* **10**, e0116589 (2015).
25. Meehan, A. L., Yang, X., McAdams, B. D., Yuan, L. & Rothman, S. M. A new mechanism for antiepileptic drug action: vesicular entry may mediate the effects of levetiracetam. *J. Neurophysiol.* **106**, 1227–1239 (2011).
26. Meehan, A. L., Yang, X., Yuan, L. L. & Rothman, S. M. Levetiracetam has an activity-dependent effect on inhibitory transmission. *Epilepsia* **53**, 469–476 (2012).
27. Dong, M. et al. SV2 is the protein receptor for botulinum neurotoxin A. *Science* **312**, 592–596 (2006).
28. Dong, M., Masuyer, G. & Stenmark, P. Botulinum and tetanus neurotoxins. *Annu Rev. Biochem* **88**, 811–837 (2019).
29. Pirazzini, M., Montecucco, C. & Rossetto, O. Toxicology and pharmacology of botulinum and tetanus neurotoxins: an update. *Arch. Toxicol.* **96**, 1521–1539 (2022).
30. Rossetto, O. & Montecucco, C. Tables of toxicity of botulinum and tetanus neurotoxins. *Toxins* **11** https://doi.org/10.3390/toxins11120686 (2019).
31. Benoit, R. M. et al. Structural basis for recognition of synaptic vesicle protein 2C by botulinum neurotoxin A. *Nature* **505**, 108–111 (2014).
32. Yao, G. et al. N-linked glycosylation of SV2 is required for binding and uptake of botulinum neurotoxin A. *Nat. Struct. Mol. Biol.* **23**, 656–662 (2016).
33. Rummel, A. et al. Botulinum neurotoxins C, E and F bind gangliosides via a conserved binding site prior to stimulation-dependent uptake with botulinum neurotoxin F utilising the three isoforms of SV2 as second receptor. *J. Neurochem* **110**, 1942–1954 (2009).
34. Peng, L., Tepp, W. H., Johnson, E. A. & Dong, M. Botulinum neurotoxin D uses synaptic vesicle protein SV2 and gangliosides as receptors. *PLoS Pathog.* **7**, e1002008 (2011).
35. Dong, M. et al. Glycosylated SV2A and SV2B mediate the entry of botulinum neurotoxin E into neurons. *Mol. Biol. Cell* **19**, 5226–5237 (2008).
36. Fu, Z., Chen, C., Barbieri, J. T., Kim, J. J. & Baldwin, M. R. Glycosylated SV2 and gangliosides as dual receptors for botulinum neurotoxin serotype F. *Biochemistry* **48**, 5631–5641 (2009).
37. Liu, Z. et al. Structural basis for botulinum neurotoxin E recognition of synaptic vesicle protein 2. *Nat. Commun.* **14**, 2338 (2023).
38. Yeh, F. L. et al. SV2 mediates entry of tetanus neurotoxin into central neurons. *PLoS Pathog.* **6**, e1001207 (2010).
39. Blum, F. C., Chen, C., Kroken, A. R. & Barbieri, J. T. Tetanus toxin and botulinum toxin a utilize unique mechanisms to enter neurons of the central nervous system. *Infect. Immun.* **80**, 1662–1669 (2012).
40. Blum, F. C., Tepp, W. H., Johnson, E. A. & Barbieri, J. T. Multiple domains of tetanus toxin direct entry into primary neurons. *Traffic* **15**, 1057–1065 (2014).
41. Chen, C., Fu, Z., Kim, J. J., Barbieri, J. T. & Baldwin, M. R. Gangliosides as high affinity receptors for tetanus neurotoxin. *J. Biol. Chem.* **284**, 26569–26577 (2009).
42. Fotinou, C. et al. The crystal structure of tetanus toxin Hc fragment complexed with a synthetic GT1b analogue suggests cross-linking between ganglioside receptors and the toxin. *J. Biol. Chem.* **276**, 32274–32281 (2001).
43. Emsley, P. et al. The structures of the H(C) fragment of tetanus toxin with carbohydrate subunit complexes provide insight into ganglioside binding. *J. Biol. Chem.* **275**, 8889–8894 (2000).
44. Masuyer, G., Conrad, J. & Stenmark, P. The structure of the tetanus toxin reveals pH-mediated domain dynamics. *EMBO Rep.* **18**, 1306–1317 (2017).
45. Megighian, A., Pirazzini, M., Fabris, F., Rossetto, O. & Montecucco, C. Tetanus and tetanus neurotoxin: From peripheral uptake to central nervous tissue targets. *J. Neurochem* **158**, 1244–1253 (2021).
46. Bercsenyi, K. et al. Tetanus toxin entry. Nidogens are therapeutic targets for the prevention of tetanus. *Science* **346**, 1118–1123 (2014).
47. Surana, S. et al. The tyrosine phosphatases LAR and PTPRδ act as receptors of the nidogen-tetanus toxin complex. *EMBO J.* **43**, 3358–3387 (2024).
48. Herreros, J., Ng, T. & Schiavo, G. Lipid rafts act as specialized domains for tetanus toxin binding and internalization into neurons. *Mol. Biol. Cell* **12**, 2947–2960 (2001).
49. Botte, M. et al. Cryo-EM structures of a LptDE transporter in complex with pro-macrobodies offer insight into lipopolysaccharide translocation. *Nat. Commun.* **13**, 1826 (2022).

50. Benoit, R. M. et al. Crystal structure of the BoNT/A2 receptor-binding domain in complex with the luminal domain of its neuronal receptor SV2C. *Sci. Rep.* **7**, 43588 (2017).
51. Gustafsson, R., Zhang, S., Masuyer, G., Dong, M. & Stenmark, P. Crystal structure of botulinum neurotoxin A2 in complex with the human protein receptor SV2C reveals plasticity in receptor binding. *Toxins* **10** https://doi.org/10.3390/toxins10040153 (2018).
52. Yamagata, A. et al. Structural basis for antiepileptic drugs and botulinum neurotoxin recognition of SV2A. *Nat. Commun.* **15**, 3027 (2024).
53. Vetting, M. W. et al. Pentapeptide repeat proteins. *Biochemistry* **45**, 1–10 (2006).
54. Zhang, R. & Kennedy, M. A. Current understanding of the structure and function of pentapeptide repeat proteins. *Biomolecules* **11** https://doi.org/10.3390/biom11050638 (2021).
55. Lazzell, D. R., Belizaire, R., Thakur, P., Sherry, D. M. & Janz, R. SV2B regulates synaptotagmin 1 by direct interaction. *J. Biol. Chem.* **279**, 52124–52131 (2004).
56. Jumper, J. et al. Highly accurate protein structure prediction with AlphaFold. *Nature* **596**, 583–589 (2021).
57. Karalewitz, A. P., Fu, Z., Baldwin, M. R., Kim, J. J. & Barbieri, J. T. Botulinum neurotoxin serotype C associates with dual ganglioside receptors to facilitate cell entry. *J. Biol. Chem.* **287**, 40806–40816 (2012).
58. Gregory, K. S., Mahadeva, T. B., Liu, S. M. & Acharya, K. R. Structural features of Clostridium botulinum neurotoxin subtype A2 cell binding domain. *Toxins* **14** https://doi.org/10.3390/toxins14050356 (2022).
59. Gregory, K. S. & Acharya, K. R. A Comprehensive structural analysis of Clostridium botulinum neurotoxin A cell-binding domain from different subtypes. *Toxins* **15** https://doi.org/10.3390/toxins15020092 (2023).
60. Mittal, A. et al. Structures of synaptic vesicle protein 2A and 2B bound to anticonvulsants. *Nat. Struct. Mol. Biol.* https://doi.org/10.1038/s41594-024-01335-1 (2024).
61. Montecucco, C. How do tetanus and botulinum toxins bind to neuronal membranes? *Trends Biochem. Sci.* **11**, 314–317 (1986).
62. Flores, A. et al. Gangliosides interact with synaptotagmin to form the high-affinity receptor complex for botulinum neurotoxin B. *Proc. Natl Acad. Sci. USA* **116**, 18098–18108 (2019).
63. Höltje, M. et al. Exchanging the minimal cell binding fragments of tetanus neurotoxin in botulinum neurotoxin A and B impacts their toxicity at the neuromuscular junction and central neurons. *Toxicon* **75**, 108–121 (2013).
64. Ho, M. et al. Recombinant botulinum neurotoxin A heavy chain-based delivery vehicles for neuronal cell targeting. *Protein Eng. Des. Sel.* **24**, 247–253 (2011).
65. Bade, S. et al. Botulinum neurotoxin type D enables cytosolic delivery of enzymatically active cargo proteins to neurones via unfolded translocation intermediates. *J. Neurochem.* **91**, 1461–1472 (2004).
66. Coen, L., Osta, R., Maury, M. & Brûlet, P. Construction of hybrid proteins that migrate retrogradely and transynaptically into the central nervous system. *Proc. Natl. Acad. Sci. USA* **94**, 9400–9405 (1997).
67. Blum, T. R. et al. Phage-assisted evolution of botulinum neurotoxin proteases with reprogrammed specificity. *Science* **371**, 803–810 (2021).
68. Dai, Y. & Lee, C. H. Transport mechanism and structural pharmacology of human urate transporter URAT1. *Cell Res.* **34**, 776–787 (2024).
69. Liu, S. et al. Recognition of antiepileptic brivaracetam by synaptic vesicle protein 2A. *Cell Discov.* **10**, 56 (2024).
70. Brunner, J. D. et al. Structural basis for ion selectivity in TMEM175 K+ channels. *eLife* **9**, e53683 (2020).
71. Brunner, J. D. & Schenck, S. Production and application of nanobodies for membrane protein structural biology. *Methods Mol. Biol.* **2127**, 167–184 (2020).
72. Sinha, K. et al. Analysis of mutants of tetanus toxin Hc fragment: ganglioside binding, cell binding and retrograde axonal transport properties. *Mol. Microbiol.* **37**, 1041–1051 (2000).
73. van der Woning, B. et al. DNA immunization combined with scFv phage display identifies antagonistic GCGR specific antibodies and reveals new epitopes on the small extracellular loops. *MAbs* **8**, 1126–1135 (2016).
74. Pardon, E. et al. A general protocol for the generation of Nanobodies for structural biology. *Nat. Protoc.* **9**, 674–693 (2014).
75. Schenck, S., Wojcik, S. M., Brose, N. & Takamori, S. A chloride conductance in VGLUT1 underlies maximal glutamate loading into synaptic vesicles. *Nat. Neurosci.* **12**, 156–162 (2009).
76. Schenck, S. et al. Generation and characterization of anti-VGLUT nanobodies acting as inhibitors of transport. *Biochemistry* **56**, 3962–3971 (2017).
77. Majd, H. et al. Screening of candidate substrates and coupling ions of transporters by thermostability shift assays. *Elife* **7** https://doi.org/10.7554/eLife.38821 (2018).
78. Mastronarde, D. N. Automated electron microscope tomography using robust prediction of specimen movements. *J. Struct. Biol.* **152**, 36–51 (2005).
79. Punjani, A., Rubinstein, J. L., Fleet, D. J. & Brubaker, M. A. cryoSPARC: algorithms for rapid unsupervised cryo-EM structure determination. *Nat. Methods* **14**, 290–296 (2017).
80. Sanchez-Garcia, R. et al. DeepEMhancer: a deep learning solution for cryo-EM volume post-processing. *Commun. Biol.* **4**, 874 (2021).
81. Afonine, P. V. et al. Real-space refinement in PHENIX for cryo-EM and crystallography. *Acta Crystallogr. D Struct. Biol.* **74**, 531–544 (2018).
82. Emsley, P., Lohkamp, B., Scott, W. G. & Cowtan, K. Features and development of Coot. *Acta Crystallogr. Sect. D., Biol. Crystallogr.* **66**, 486–501 (2010).
83. Pettersen, E. F. et al. UCSF ChimeraX: structure visualization for researchers, educators, and developers. *Protein Sci.* **30**, 70–82 (2021).

Acknowledgements

We thank the nanobody discovery team at the VIB-VUB Center for Structural Biology for their work and the nanobody cDNAs. We thank Dr. Yves Nerinckx (AFSCA) and his co-workers from the Abattoir of Brussels for supply with fresh lamb brains. We are grateful to Drs. Marcus Fislage (Biogenic Electron Cryo-Microscopy (BECM), Brussels) and Dirk Reiter (VIB-VUB Center for Structural Biology, Brussels) for assistance with cryo-EM data collection and technical support for workstations and IT-related questions, respectively. We thank Prof. Damya Laoui (VIB-VUB Center for Inflammation Research, Brussels) for mouse brains. We would like to acknowledge the funding provided by Vlaams Instituut voor Biotechnologie (VIB) to J.D.B. and to J.S.

Author contributions

S.S. and J.D.B. conceived the study and planned experiments; S.S. expressed and purified proteins, formed the complexes, prepared samples for cryo-EM, and performed DSF experiments; T.L. and J.S. performed the nanobody discovery; J.D.B. prepared grids for cryo-EM, collected and processed cryo-EM data and built the models; S.S. and J.D.B. analyzed data and wrote the manuscript.

Competing interests

The authors declare no competing interests.

Additional information

Supplementary information The online version contains supplementary material available at https://doi.org/10.1038/s41467-025-59545-0.

Correspondence and requests for materials should be addressed to Janine D. Brunner.

Peer review information *Nature Communications* thanks the anonymous reviewers for their contribution to the peer review of this work. A peer review file is available.